

Chapter IV

Sensor Models

In Chapter III, we covered a variety of methods for modeling images. For some special types of imagery, a simple physics-based image-generating mechanism is available, but this is the exception rather than the rule.

This chapter focuses on statistical models for the devices that acquire images – e.g., cameras. Here fairly accurate physics-based models are generally available. We provide an overview of these models, focusing the exposition on photographic film and solid-state cameras.

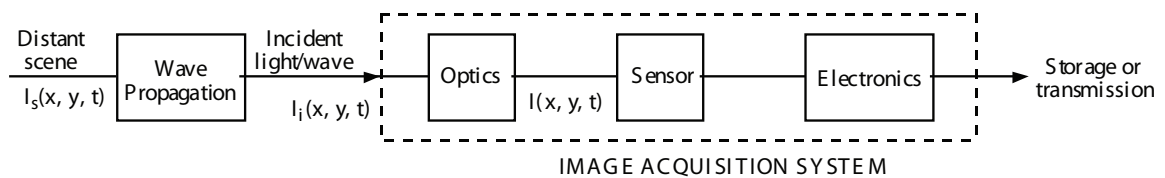


Figure 1: Block-diagram of image acquisition system.

A generic image acquisition model is shown in Fig. 1. It features the following components:

- *Propagation effects*, including atmospheric turbulence. Such effects are usually negligible, with the exception of a few special applications (e.g., some types of astronomical imagery, and imagery from polluted environments).
- *Optics*: often modeled as linear shift-invariant blur. Note however that chromatic aberrations are more accurately modeled using linear shift-variant models.
- *Sensors*: they convert light into a recordable quantity (such as exposed photographic film, electric charges, or electric current). The sensor output is usually nonlinear in the incident light intensity, and contains noise due to the quantum nature of light and various sensor imperfections.
- *Electronic circuitry*: this is a source of thermal noise which is generally well modeled by additive white Gaussian noise.

Often digitization is integrated into the image acquisition system, producing quantization noise or more generally, compression noise (e.g., for images output in JPEG format).

In the last ten years there have been considerable advances in the development of smart sensors. These are sensors that also perform image processing operations on the substrate where the sensor is located.

1 Photographic film

We begin our study with photographic film. This venerable technology has seen its share of technological developments over time. The material below is a summary of [1, Ch. 2.7].

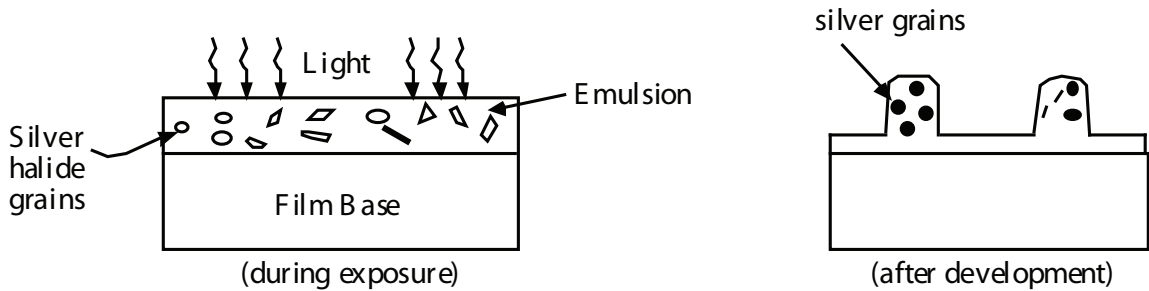


Figure 2: Exposure and development of film.

Referring to Fig. 2, a film consists of a photosensitive emulsion layer and a transparent plastic base whose sole purpose is to provide mechanical support to the emulsion layer. A typical emulsion layer is 5–25 μm thick and is made of silver salt grains embedded in gelatin. The silver halide grains are photosensitive. When a grain absorbs a photon, one or more molecules are reduced to silver, and the grain becomes exposed. The exposure at location (x, y) is the integral of the incident illumination during the aperture time:

$$E(x, y) = \int_0^{T_{ap}} I(x, y, t) dt.$$

Film development reduces silver halide grains to silver. This is a chemical reaction which proceeds much more rapidly on exposed grains than on nonexposed ones. At some point, unreduced grains are washed off the base. What remains is a granular silver coating of varying thickness $D(x, y)$. For a range of values of the exposure E , the density D is approximately a linear function of $\log E$, see Fig. 3. The slope of this linear segment is the gamma (γ) of the curve.

The choice of a particular type of film is a compromise between resolution, sensitivity (to low light levels) and maximum density. With current film technology, a single photon might suffice to expose a grain. Therefore large grain sizes are preferred when lighting conditions are

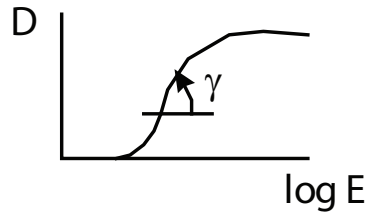


Figure 3: $D - \log E$ curve (or H and D curve, from Hurter and Driffield).

poor or when high-speed photography is needed – both resulting in low exposure. Conversely, fine grain is desirable for high-resolution images, e.g., for portraits and landscapes.

Statistical Model: Due to the random location of the silver grains and the quantum nature of light, the image on film is not $D(x, y)$ but may be thought of as a doubly stochastic process $f(x, y)$ whose statistics are governed by grain geometry and by a spatial Poisson process with intensity $\log E(x, y)$ — see Fig. 4 for an example. Consider a cell at location (x, y) which is small enough so that $\log E(x, y)$ may be regarded as a constant over the cell, yet is large enough to include many developed grains. Using a high-count approximation ($\log E(x, y) \gg 1$), we model the average image intensity over the cell as

$$\bar{f}(x, y) \sim \gamma \log E(x, y) + \sqrt{\gamma \log E(x, y)} w(x, y)$$

where $w(x, y)$ is spatially white Gaussian noise with mean zero and unit variance. Hence, the noise is signal-dependent, with variance equal to $\gamma \log E(x, y)$.



Figure 4: Grainy negative $f(x, y)$ from high-speed black-and-white film.

2 Solid-state imaging

The first digital camera was developed by Kodak laboratories in 1973. It had 10,000 pixels, was monochrome, had an aperture time of 23 seconds, and was of course never commercialized. The first commercial products (for professional use) appeared in 1988, but it was not until 1995 that digital cameras became popular on the consumer market.

We focus our discussion on Charged Coupled Device (CCD) arrays. These devices are used in modern TV cameras, mass-market digital cameras, astronomical imaging, hyperspectral cameras, and fax scanners. CCD arrays exist in a great variety of spatial resolution and exposure times. Less common are Complementary Metal-Oxide Semiconductor (CMOS) sensors despite some technological advantages: lower noise and lower heat dissipation.

2.1 Noise-Free Model

The basic properties of a CCD camera can be understood by first neglecting noise and other imperfections in the sensors. Fig. 5 depicts four cells of a CCD array and the conversion of the incident, time-varying light field $I(x, y, t)$ to an electric charge $c(n, m)$ stored in each cell (n, m) . We have

$$c(n, m) = \int_0^{T_{ap}} \int_{C_{nm}} I(x, y, t) dx dy dt$$

where T_{ap} is the aperture time of the camera and C_{nm} denotes cell (n, m) of the CCD array.

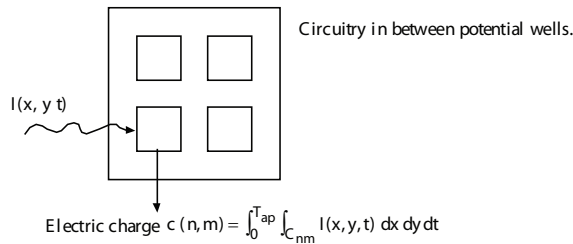


Figure 5: Conversion of light field $I(x, y, t)$ to electric charges $c(n, m)$ for individual cells of a CCD array.

Equivalently, we may write

$$c(n, m) = (E \star h)(nT_1, mT_2)$$

where T_1 and T_2 are the sampling periods,

$$E(x, y) = \int_0^{T_{ap}} I(x, y, t) dt$$

is the exposure, and $h(x, y)$ is the sampling aperture (here a box function).

Note: The ideal *frequency response* of $h(x, y)$ should be 1 over the rectangle

$$\left[-\frac{1}{2T_1}, \frac{1}{2T_1}\right] \times \left[-\frac{1}{2T_2}, \frac{1}{2T_2}\right],$$

so the sampling aperture actually used, which has sinc frequency response, is undesirable. To compensate for the poor attenuation of highpass frequencies (which may result in annoying aliasing artifacts), one needs to slightly defocus the camera — in essence, implementing an optical antialiasing filter.

2.2 Statistical Model

We now present a more refined model of the photoconversion process, which takes into account the quantum nature of light as well as various sensor imperfections [2].

Let us start with a simple model capturing basic quantum effects. Denote by $c(n, m)$ the number of photons landing in cell C_{nm} and converted into photoelectrons. This is a Poisson random variable with intensity

$$\lambda(n, m) = \int_{C_{nm}} E(x, y) dx dy.$$

This model is more appropriate than that of Sec. 2.1 for low-count imaging applications such as imaging of faint, distant stars, and nuclear medicine.

Several simplifications of this model could be considered. For high-count imaging, one can use the Gaussian approximation

$$c(n, m) \sim \lambda(n, m) + \sqrt{\lambda(n, m)} w(n, m)$$

where $w(n, m)$ is zero-mean, unit-variance white Gaussian noise. For very high count imaging, one can simply ignore quantum effects and use the approximation

$$c(n, m) \sim \lambda(n, m)$$

which is in effect the approach followed in Sec. 2.1.

Modeling $c(n, m)$ as a Poisson random variable with intensity $\lambda(n, m)$ assumes perfect photon to electron conversion. In reality, charge-transfer efficiency is imperfect and is not even uniform across the CCD array. There might even be “dead pixels”, which are insensitive to incident light. These factors may be modeled by introducing an efficiency factor $\beta(n, m) \in [0, 1]$ for the photoconversion process in each cell. Then $c(n, m)$ is viewed as a Poisson random variable with parameter $\beta(n, m)\lambda(n, m)$.

Additionally, there is a spurious generation of photoelectrons due to

- background radiation on CCD chip;
- dark current (spontaneous generation of electrons due to heat);
- bias (imperfect calibration).

Finally, in addition to the quantum effects, thermal noise and bias in amplifier in electronics (readout noise) add a $\mathcal{N}(0, \sigma^2)$ term to the measurements.

Taking all of the above effects into account, we obtain the following model:

$$c(n, m) = \text{Poisson}[\beta(n, m)\lambda(n, m) + \lambda_{\text{back}}(n, m) + \lambda_{\text{dark}}(n, m) + \lambda_{\text{bias}}(n, m)] + \mathcal{N}(0, \sigma^2).$$

This model has been successfully used to restore blurred, photon-limited image data from the Hubble space telescope [2].

2.3 Color CCD arrays

The goal here is to acquire the R, G, B components of a color image. The most common technical solution is to form all three images on the same CCD chip.

A color filter array is overlaid on top of a monochrome CCD array. There are three types of filters, with sensitivity responses $S_R(\nu)$, $S_G(\nu)$, and $S_B(\nu)$ given as a function of optical frequency ν . The color pixels are given by

$$\begin{aligned} R(n, m) &= \int S_R(\nu)I(n, m, \nu) d\nu \\ G(n, m) &= \int S_G(\nu)I(n, m, \nu) d\nu \\ B(n, m) &= \int S_B(\nu)I(n, m, \nu) d\nu \end{aligned}$$

A popular configuration of color pixels is the Bayer mosaic shown in Fig. 6. Once the color pixels in the Bayer mosaic have been obtained, the following operations are performed:

- interpolate R, G, B images to get color pixels at high resolution. This operation is also called *demosaicing* [3]
- convert to another color space, e.g., YC_rC_b .

One disadvantage of this technology is the use of color filters, which pass one color and absorb the other two. In effect, this reduces the SNR.

Another method consists of using three CCD arrays (one for each color component). The color components of incoming light are separated via a dichroic prism, see Fig. 7. This technology provides high quality but is expensive.

A third method consists of layering (stacking) the photosensors. The Foveon X3 sensor has the blue layer at the top, green below, and red at the bottom. There is some diffusion of photoelectrons at the bottom, hence a slight reduction of sharpness for the red image.

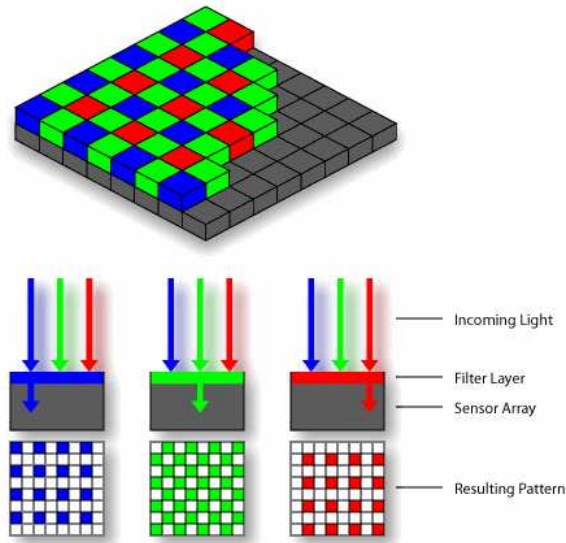


Figure 6: Bayer mosaic.

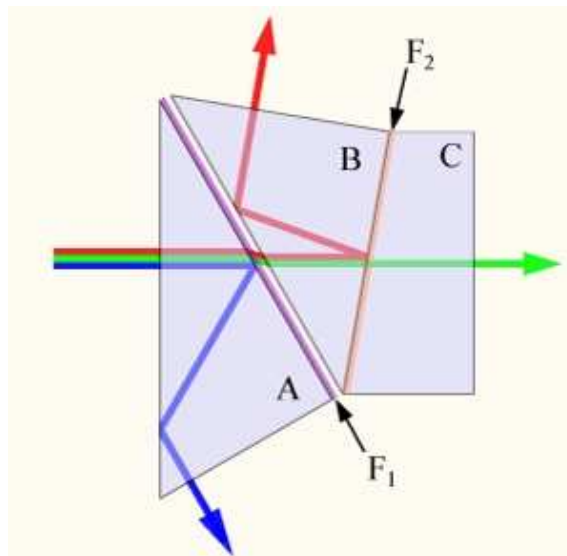


Figure 7: Separation of color components of light using dichroic prism.

References

- [1] K. R. Castleman, *Digital Image Processing*, Prentice-Hall, 1996.
- [2] D. L. Snyder, A. M. Hammoud, and R. L. White, "Image Recovery from Data Acquired with a Charge-Coupled-Device Camera," *J. Opt. Soc. Am. A.*, Vol. 10, No. 5, pp. 1014-1023, May 1993.
- [3] P. Vora and C. Herley, "Trade-offs Between Color Saturation and Noise Sensitivity in Image Sensors," *Proc. 5th IEEE Int. Conf. on Image Proc. (ICIP 98)*, Chicago, IL, Oct. 1998.